Copyright © 2009 American Scientific Publishers
All rights reserved
Printed in the United States of America

Nanoscience and Nanotechnology Letters
Vol. 1, 111–118, 2009

Fabrication of Nanodielectric $BaTiO_3$ Composites Exhibiting Stable Capacitor Functions in the High Frequency (>100 MHz) Through Interfacial Polarization Interactions

A. Biswas[1,*], I. S. Bayer[2,*], A. Tripathi[3], E. H. Lock[4,†], S. G. Walton[4], M. G. Norton[5], D. K. Avasthi[3], D. H. Dahanayaka[1], L. A. Bumm[1], E. Suhir[6], A. R. Chowdhury[7], and R. Gupta[8]

[1] *Center for Semiconductor Physics in Nanostructures, Department of Physics and Astronomy, University of Oklahoma, Norman, OK 73019, USA*
[2] *Department of Aerospace Engineering, University of Illinois at Urbana-Champaign, IL 61801, USA*
[3] *Inter University Accelerator Center (IUAC), New Delhi 110067, India*
[4] *Plasma Physics Division, Naval Research Laboratory, Washington 20375, DC, USA*
[5] *School of Mechanical and Materials Engineering, Washington State University, Pullman, Washington 99164, USA*
[6] *Department of Electrical Engineering, University of California, Santa Cruz, California 95064, USA*
[7] *Department of Physics, University of Alaska, Fairbanks, AK 99709, USA*
[8] *Department of Physics, University of Petroleum and Energy Studies, Dehradun 248006, India*

Delivered by Publishing Technology
to: University of Oklahoma
IP: 129.15.7.47 On: Wed, 17 Feb 2010 16:25:49

We report fabrication of two different nanodielectric composites comprising a uniform blend of inorganic–organic and inorganic–inorganic dielectric materials by a simple and single-step method of electron-beam-assisted vapor-phase codeposition. The fabrication method allowed ambient temperature (~35 °C) generation of well-crystallized ultra-fine (~5 nm) to relatively larger (~150 nm) barium titanate BTO nanoparticles in lithium fluoride (LiF) and poly(methylmethacrylate) (PMMA) dielectric matrices. No high temperature sintering was performed. The fabricated nanodielectric composites showed unique nanometric interfacial polarization properties that resulted in very promising high-frequency (>100 MHz) capacitor functions. The challenges of ferroelectric losses in the high-frequency were overcome and attributed to the possible interplay of polarization mechanisms contributed by the dielectric elements of nanostructured composites that allowed a frequency-independent capacitor performance. The best capacitor performance was achieved from as-deposited BTO-LiF nanodielectric systems that exhibited a flat capacitance density of about 10 nF/cm^2 with the self resonance frequency occurring at around 150 MHz along with a low loss tangent of about 0.1 at 100 MHz, thus verifying the high-quality of the device structures. The fabricated nanodielectric composites may be suitable for a variety of high-frequency applications in miniaturized electronic systems.

Keywords: Nanodielectric Composites, Ferroelectric Nanoparticles, Vapor-Phase Codeposition, Capacitors, Electronic Miniaturization, Dielectric Constant.

1. INTRODUCTION

Nanostructured composites comprising ferroelectric oxide nanoparticles (<200 nm) dispersed in organic or inorganic matrices have recently emerged as promising advanced electronic materials due to their novel dielectric properties.[1–3] Such materials, so called nanodielectric composites allow combination of structurally, electronically or chemically different phases of dielectric materials at the nanoscale.

The surfaces and interfaces between dielectric elements of nanodielectric composites become increasingly prominent as the ferroelectric particles shrink in size to nanometric scale, and the important properties such as degree

*Authors to whom correspondence should be addressed.
†NRL/NRC Postdoctoral Research Associate.

of polarization and charge separation are dominated by the interfacial interactions of the particles with the matrix.[1] This results in unique interfacial polarization properties that can be leveraged to overcome some of the performance constraints that conventional ferroelectric materials exhibit in the radio frequency (>1 MHz). For example, conventional ferroelectric materials exhibit dielectric relaxation as a result of alterations of the elastic and electric behavior and the movement of the domain walls at frequencies exceeding 1 MHz.[4] While high specific capacitance (i.e., capacitance density) can be obtained from these materials, dielectric relaxation limits their stable capacitor performance in the high-frequency.

Nanodielectric composites offer the possibility to incorporate high specific capacitance and frequency-independent capacitor function concurrently in one material. Nanometric interfacial interactions between the ferroelectric nanoparticles and the dielectric matrix can significantly influence the degree of polarization. The resulting interplay of polarization mechanisms can dramatically improve the dielectric relaxation behavior in the high-frequency.[5]

Engineering of such unique nanometric interfacial properties of nanodielectric materials requires composite fabrication capability to precisely blend, tailor and optimize several materials at the nanoscale in one material. This simultaneously creates opportunities for addressing a wide range of both active and passive advanced electronic applications. Capacitive components that are light-weight, volume-efficient, flexible and high-performance (i.e., high specific capacitance together with stable capacitor functions) are needed for high-frequency (>1 MHz) miniature electronic systems for various functional applications. These include energy storage, ultrasensitive transducers, embedded capacitors as well as nanoelectromechanical systems (NEMS).[2, 4–10]

In this paper, we present fabrication, structural and electrical characterization results of two different nanodielectric composites comprising BTO nanograins (5–150 nm) dispersed in polymethyl(methacrylate) (PMMA) and lithium fluoride (LiF) matrices. Our research was driven by the motivation to fabricate nanodielectric composites by combining a variety of dielectric materials in order to gain knowledge of the role of interface on the degree of polarization and the resulting capacitor functions in the high frequency (>100 MHz) region. The composites were fabricated by an ambient temperature (~35 °C) vacuum codeposition method that did not require high temperature sintering to crystallize BTO. It is noteworthy here, that a low temperature processing of crystalline BTO nanoparticles is very important in order to facilitate development of organic substrate-based flexible capacitors that are needed for many applications in the next generation of electronics. We discuss the comparative capacitor performances of the fabricated composites in the high-frequency (>100 MHz).

2. EXPERIMENTAL DETAILS

2.1. Fabrication and Characterization of Nanostructured BTO Composites

Composites were fabricated by a solvent-free method based on electron-beam (e-beam)-assisted vapor-phase codeposition in vacuum that allows single-step ambient temperature fabrication of composites comprising BT nanoparticles in PMMA and LiF matrices. Simultaneous evaporation of BTO (99.9% pure granulates, Alfa Aesar) and PMMA (granulates, Alfa Aesar), and BTO and LiF (fine powder, Alfa Aesar) were carried out in a high-vacuum codeposition system that contains a four-pocket e-beam source. The details of the codeposition system are given in our earlier publication.[11] Composites of different thicknesses (approximately 100 nm and 500 nm) were fabricated onto carbon coated TEM grids and Al-sputter-coated Si substrates respectively. Composites with a good degree of uniform dispersion along with fairly high volume filling (~60%) of BTO nanoparticles in different matrices were fabricated. Thicker composites were used for electrical characterizations. The substrate temperature during deposition was about 35 °C. A quartz crystal microbalance thickness monitoring unit installed in the deposition chamber was used to monitor the deposition rates and measuring the thickness of the composites. Profilometer measurements were also carried out to determine the thickness of the fabricated composites.

The samples were annealed at 130 °C, which is above the Curie temperature of BTO (120 °C), to investigate the effects of thermal stress on capacitance values. An *LCR* meter (HP4286A rf) was used to measure the capacitance of the composites as a function of frequency. X-ray diffraction (XRD) and atomic force microscopy (AFM) were carried out using a Brucker D8 Advance Diffractometer with a Cu K_α line and a digital multimode scanning probe microscope with Nanoscope IIIa controller, respectively. Sample morphology was also studied by a transmission electron microscope (TEM) using a Philips CM 200 operated at 200 kV.

3. RESULTS AND DISCUSSION

3.1. Ultra-Fine Cubic BTO Nanoparticles in PMMA Matrix

We fabricated thin (~100 nm) and thicker (~500 nm) composites comprising ultrafine (<5 nm) and relatively larger (~100 nm) BTO nanoparticles respectively. Figure 1(a) shows a TEM image of a nanocomposite of thickness of about 100 nm comprising networks of BTO nanoparticles in a PMMA matrix. The dark and light contrast regions correspond to the polymer and BTO respectively. The nanocomposite structural morphology reveals interesting nanoscale features comprising networks

Delivered by Ingenta to: University of Notre Dame IP : 129.74.171.57 Wed, 24 Feb 2010 16:57:05

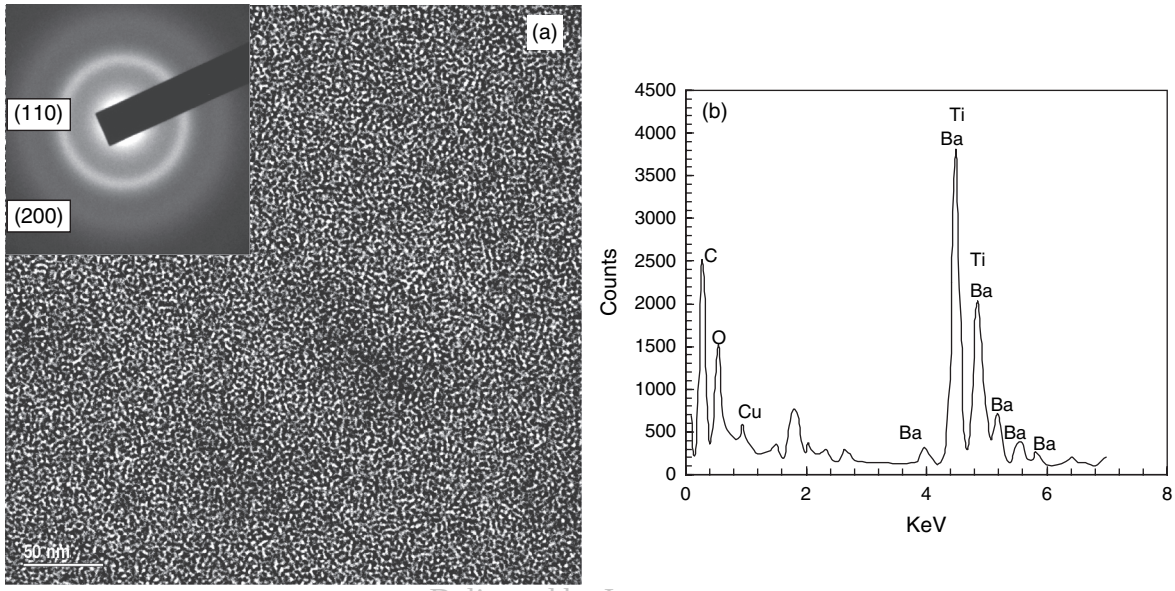

Fig. 1. TEM image of a BTO/PMMA nanocomposite with EDX spectrum showing barium and titanium peaks. Inset shows the SAED patterns of BTO nanoparticles.

Delivered by Ingenta to:
University of Notre Dame
IP : 129.74.171.77
Wed, 24 Feb 2010 16:57:05

of ultra-fine BTO nanoparticles of size of about 5 nm embedded in the PMMA matrix. Figure 1(b) shows the TEM energy dispersive X-ray (EDX) spectra of elemental profile of the nanocomposite. The inset of Figure 1(a) shows the TEM selected area diffraction pattern (SAED) of BTO nanoparticles. The diffraction patterns comprising a (110) and a weak (200) correspond to a cubic structure of the ultra-fine BTO nanostructures. Cubic phase is considered the usual crystal structure in ultra-fine BTO nanoparticles.[12]

In the following section, we present XRD results of the thicker composites comprising larger BTO nanoparticles that indicate presence of both tetragonal and cubic phases.

3.2. AFM and XRD Investigations of BTO/PMMA and BTO/LiF Nanostructured Composites

Figure 2 shows AFM images of as-deposited and annealed BTO/PMMA and BTO/LiF composites of thickness of about 500 nm. Figures 2(a) and (b) show surface topography images of as-deposited BTO/PMMA and BTO/LiF samples respectively. They indicate a high-degree of uniform dispersion of BTO nanograins of diameter ranging from about 50 nm to 100 nm in PMMA. On the other hand, relatively larger BTO particles of about 150 nm in LiF matrices can be seen in Figure 2(b). Annealing the samples resulted in interesting structural morphologies due to coalescence and BTO grain growth. Figure 2(c) shows AFM surface topography of an annealed BTO/PMMA sample. The morphology can be described as individually assembled BTO nanograins/nanoparticles held together within the polymer matrix. These form irregularly shaped clusters that give rise to a percolating structure and at the same time, changing the filling factor of the original thin film composites. This is similar to our earlier observation of characteristic percolating polymer-metal nanocomposite with very high metal nanoparticle volume fillings.[13] Similarly, AFM topography of an annealed BTO/LiF sample also indicates formation of large clumps of coalesced BTO particles (Fig. 2(d)). The shape of the BTO nanograins also appear to be more spheroidal upon annealing compared to somewhat faceted BTO structures present in as deposited BTO/LiF samples (Figs. 2(b and d)).

The XRD spectra of the PMMA and LiF based composite systems showed coexistence of tetragonal and cubic phases of as-deposited BTO as shown in Figure 3(a). Major cubic (paraelectric) and tetragonal (ferroelectric) phases of BTO are assigned as (100), (111), (200), (210), (211) and (002).[14] However, for BTO/LiF system, a more dominating cubic structure is observed. This may be attributed to the cubic structure of LiF matrix, and the short-range and long-range exchange coupling in crystalline phases between the BTO and the LiF. The peaks at around 38° (111) and 45° (200) may be attributed to the cubic LiF matrix.[15] Further, the peak around 42° (**) indicates the possibility of the formation of the compound BaF_2, which is also cubic.[16]

For both BTO/PMMA and BTO/LiF composite systems, multiple peaks around 36° (***) are also detected (Fig. 3(a)), which might be due to ferroelectric $BaTi_2O_5$.[17] Further, a small peak around 43° (*) in the XRD of BTO/PMMA may have emerged due to a by-product $BaCO_3$.[18] These peaks, i.e., (*), (**) and (***) are broader possibly indicating oriented poly-crystalline properties, while the sharp peaks indicate that the film had single-crystalline morphology. In Figure 3(b), XRD spectra of the annealed composites are shown. No additional peaks

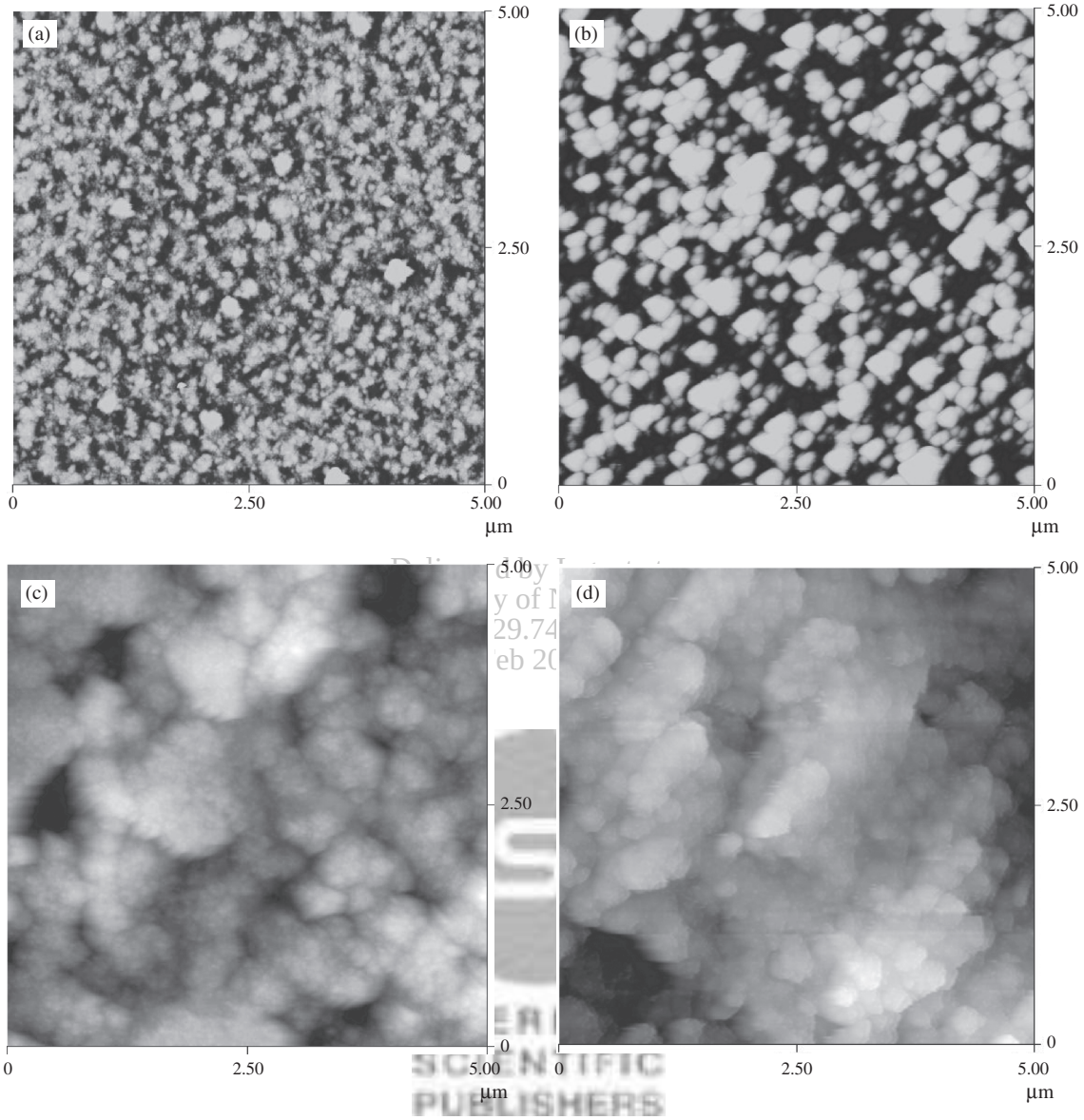

Fig. 2. AFM montages: surface topography of the as-deposited BTO/PMMA and BTO/LiF nanostructured composites (a) and (b). (c) and (d) show surface topography of annealed BTO/PMMA and BTO/LiF samples respectively. All images are 5 μm × 5 μm.

are observed related to the crystalline properties of the BTO/LiF composites consistent with our expectation that annealing to 130 °C would'nt alter the crystalline morphology of the BTO/LiF ceramics. In the case of BTO/PMMA, although the BTO particles coalesced highly upon annealing, the crystallographic signature in Figure 3(b) has not practically changed. This might suggest that the coalesced particles did not fuse into one another but rather closely packed in clumps of 5 μm or larger as the AFM images in Figure 2 indicate. A similar argument could be considered for the annealed BTO/LiF composites. The presence of impurity phases is still observed in the XRD data of the annealed films. It is important to note that such impurities and poly-crystalline structures dominate the dielectric response of the composite films at radio frequencies.

3.3. High-Frequency Capacitor Functions

Figure 4 shows capacitance density as a function of frequency along with loss tangent data of as-deposited and annealed (130 °C) BTO-PMMA composites. As-deposited composites exhibited a very stable and a capacitance density of ∼12 nF/cm^2 with a resonance frequency occurring at around 80 MHz (Fig. 4(a)) along with a loss tangent of about 0.5 (Fig. 4(c)). The stable capacitor behavior with the changing field may be probably due to the contributions of polarization modes of BTO and PMMA that apparently balance each other in responding to the changing electric field at radio frequency, thus preventing occurrence of an earlier ferroelectric loss due to the BTO particles.[10] Annealing the composites at 130 °C above the Curie temperature of BTO (120 °C) and the glass transition temperature

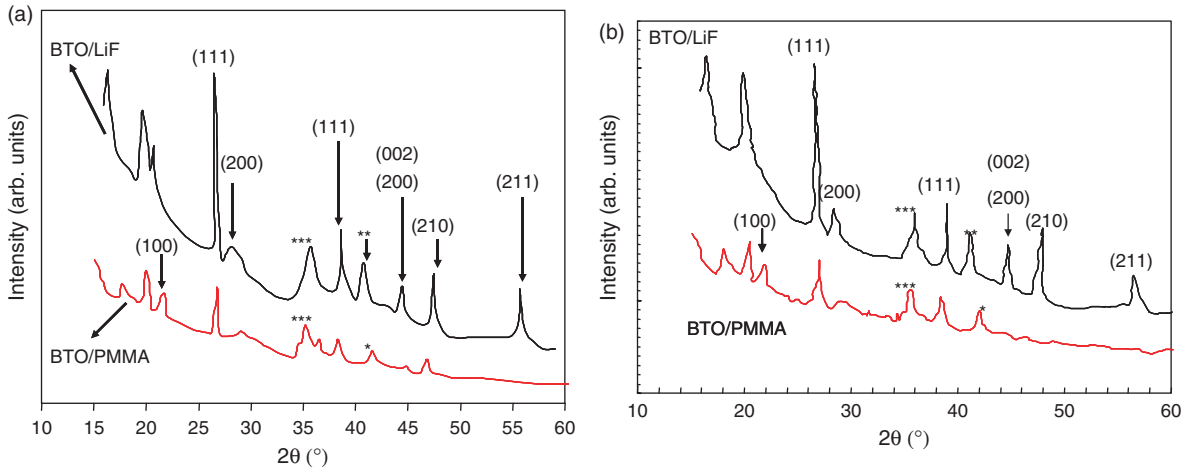

Fig. 3. X-ray diffractograms of the as-deposited (a) and annealed (b) BTO/LiF and BTO/PMMA composites.

of PMMA (∼100 °C),[19] resulted in a decrease in the capacitance density of 1.2 nF/cm^2. However, of particular significance is the shift of dielectric relaxation into the higher frequency region with the self resonance occurring at around 410 MHz (Fig. 4(b)). A low loss behavior (loss tangent of about 0.07) is also observed up to 200 MHz frequency (Fig. 4(d)). Dielectric constant versus frequency plots of the fabricated composites are given in Figure 5.

As reported in our earlier work,[10] the loss of ferroelectricity and the decrease in capacitance density of the annealed BTO-PMMA composites may be attributed to the transformation of ferroelectric phase of BTO into a dominant paraelectric phase upon annealing the composites above the Curie point of BTO. Apart from this phase transformation effect, the change in size and connectivity (clump formation) of the BTO particles after annealing

Delivered by Ingenta to:
University of Notre Dame
IP: 129.74.1.17
Wed, 24 Feb 2010 16:07:07

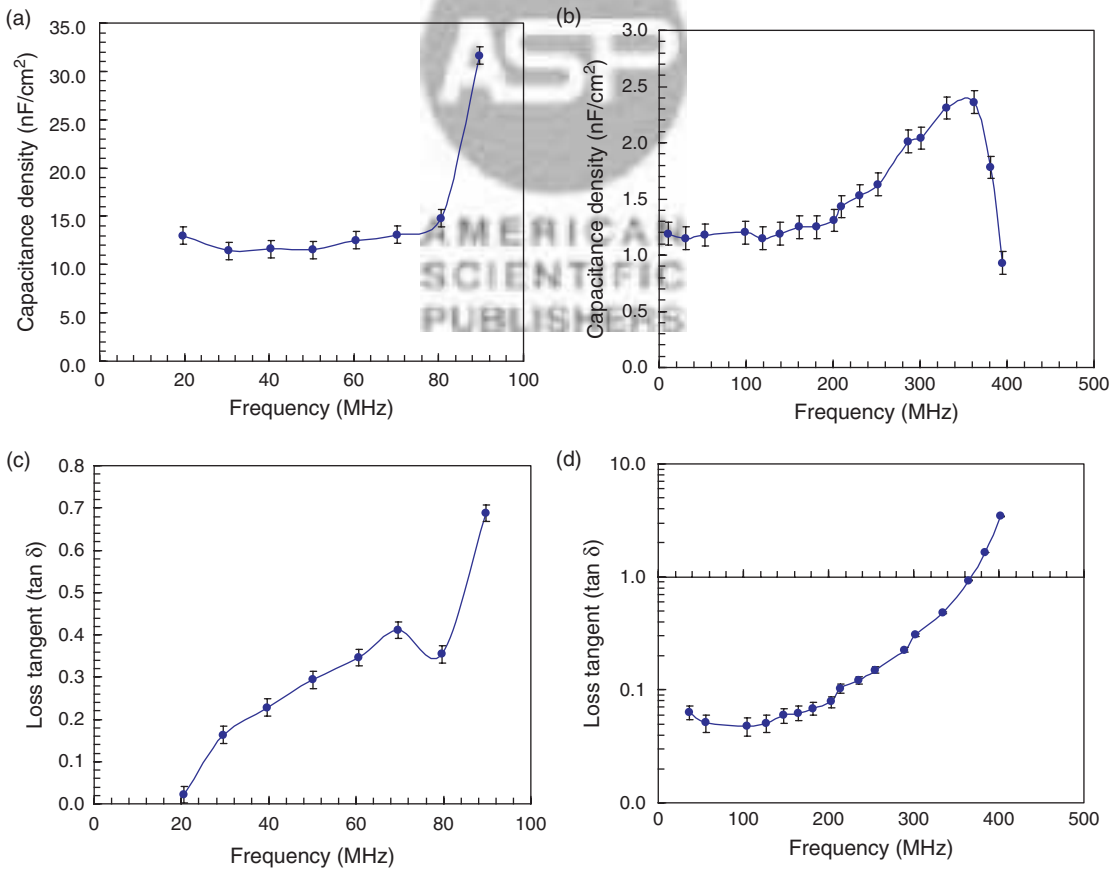

Fig. 4. Capacitance density–frequency response and the corresponding loss tangent tan δ of the as-deposited (a) and (c) and annealed BTO/PMMA composites (b) and (d).

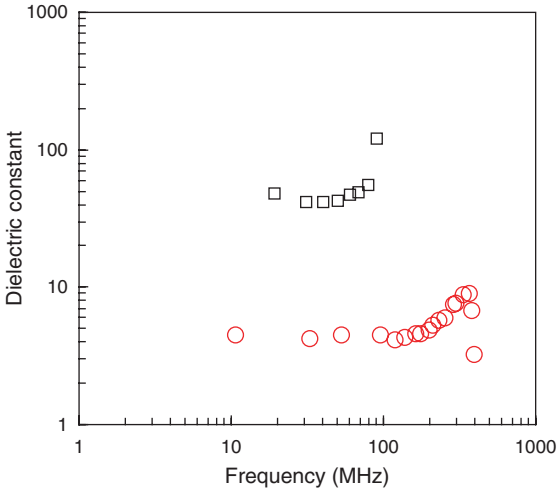

Fig. 5. Dielectric constant versus frequency log–log plot for as deposited (squares) and annealed (circles) BTO/PMMA composites shown in Figure 4.

Delivered by Ingenta to:
University of Notre Dame
IP: 129.74.17.177
Wed, 24 Feb 2010 16:57:05

(Fig. 2(c)) might also have affected the dielectric properties of the BTO/PMMA composites.

We observe a significant shift of dielectric relaxation in the higher frequency (~410 MHz) upon annealing BTO/PMMA composites. This notable shift of dielectric relaxation may be due to the minimization of ferroelectric losses.[10] In our earlier work on BTO/PANI-PU nanocompisites, we observed a dielectric relaxation shift and self resonance frequency occurring at around 200 MHz upon annealing.[10] Since the organic matrix is different in the present case, we also consider here the possible contribution of the modified PMMA matrix (i.e., the modified interface) in improving the dielectric relaxation and self resonance frequency of the composite. It has been observed that heating PMMA above 100 °C (glassy-to-rubbery transition) enhances the mobility of the polymer segments and facilitates dipole self-organization. This in turn, has been found to result in an increase of the relative permittivity up to two orders of magnitude.[19] The higher relative permittivity would allow for more degrees of freedom for electric dipoles (orientation polarization). As the dielectric relaxation is a strong function of the alignment of dipoles with respect to polymer chain segments,[20] we argue that the contribution of the polarization mode from modified PMMA matrix with enhanced permittivity may have prevented the occurrence of an earlier self resonance frequency and shifted the overall dielectric relaxation of the composite to the higher frequency region. The current–voltage characteristics (I/V) data of annealed composites (not shown here) exhibited a much less lossy medium compared to the as-deposited composites.

The BTO-LiF composites were annealed at two different temperatures—below and above Curie point of BTO in order to study the corresponding capacitor performance. As-deposited composites exhibited a nearly flat capacitance density of about 10 nF/cm^2 up to 100 MHz (Fig. 6(a), BaLiF-3).

Annealing the composites at 70 °C did not result in appreciable change in the capacitance density (Fig. 6(a), BaLiF-2). Further, the as-prepared composites and composites annealed at 70 °C exhibited fairly low dissipation factors (loss tangent) of about 0.1 at 100 MHz. The low loss capacitor behavior even at such a high frequency is surprising, particularly in view of relatively high dielectric constant of LiF (9.036) [21] when compared to PMMA (3.2 @ 1 MHz).[22] Relatively high dielectric constant materials such as LiF are usually expected to produce high dissipation factors in the changing electric field. In order to understand the capacitor performance, we consider the possible interplay of respective ionic polarization originating from both BTO and LiF. Short range and long range ionic–ionic polarization interactions are possible in the present case with the uniformly dispersed BTO nanoparticles in LiF, which induces a fast polarization in the composite material compatible with the changing electric field. We also present dielectric constant-frequency data for the BTO/LiF composites shown in Figure 7.

Annealing at 130 °C beyond the Curie temperature of BTO (paraelectric phase) resulted in a decrease in the

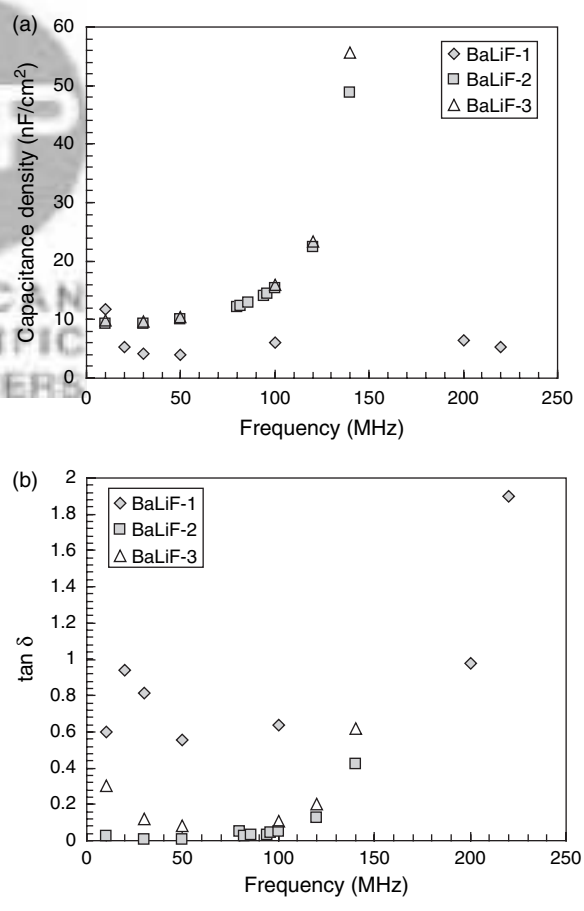

Fig. 6. Capacitance density–frequency response, (a) and the corresponding loss tangent tan δ, (b), of the as-deposited and annealed BTO/LiF composites.

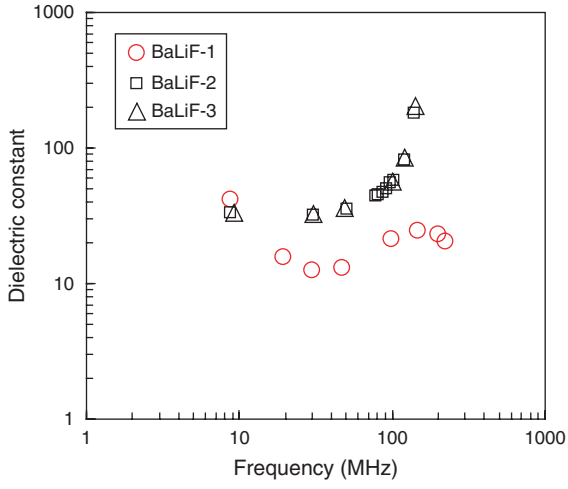

Fig. 7. Dielectric constant versus frequency log–log plot for the as-deposited and annealed BTO/LiF composites.

capacitance density of about 4 nF/cm^2 with the resonance frequency occurring around 200 MHz (Fig. 6(a), BaLiF-1). Notable is the high loss tangent of about 0.6 occurring at around 100 MHz (Fig. 5(b), BaLiF-1). The temperature has a complicated influence on the dielectric properties of LiF. It has been observed that increasing temperature of LiF above 100 °C increases its dielectric constant and the loss tangent.[22] Increasing temperature can increase the ionic distances, which in turn can affect the ionic and electronic polarizations resulting in a very high loss tangent.[22] In a recent study,[23] a very complicated temperature effect on the loss tangent of LiF doped barium iron niobate composites were observed particularly at LiF concentrations below 4%. Both the dielectric constant and loss tangent showed an increasing trend above annealing temperatures of 130 °C at 1 kHz. Although the results in Figure 5 do not clearly distinguish between the effects of paraelectric/ferroelectric and morphological transformations, the morphological changes observed upon annealing (Fig. 2) on both BTO-in-polymer and BTO-in-LiF composites have a deterministic effect on the electronic and ionic polarization efficiencies of the films which are reflected in the radio frequency dielectric constant and loss tangent. It should also be noted that the existing impurities as evidenced by the XRD data of Figure 3, can interfere with the dielectric response of the nanostructured films. The fabricated BTO nanostructured dielectric composites could be promising as high-performance, light weight and volume-efficient thin film capacitors for a variety of applications in high-frequency miniature electronic devices including portable communication systems.

4. CONCLUSIONS

We have fabricated ultra-thin (~100 nm) and thicker (~500 nm) nanodielectric composites comprising ferroelectric barium titanate (BTO) nanoparticles uniformly dispersed in lithium fluoride (LiF) and poly(methylmethacrylate) (PMMA) matrices by a simple and single-step method of electron-beam-assisted vapor-phase co-deposition. The ambient temperature (~35 °C) fabrication method allowed production of well-crystallized BTO nanoparticles that did not require thermal treatment to induce crystallinity in BTO. While, ultra-fine BTO nanoparticles (~5 nm) showed a cubic crystalline structure, larger BTO particles (~50 nm–150 nm) indicated co-existence of cubic and tetragonal phases. The fabricated nanostructured composites exhibited very promising capacitor functions in the high frequency (>100 MHz). As-deposited ceramic-in polymer and ceramic-in-insulator nanodielectric composites exhibited capacitance density of 12 nF/cm^2 and 10 nF/cm^2 with resonance frequency close to 100 MHz and 150 MHz, and with loss tangent of 0.8 and 0.1 respectively. Annealing composites at 130 °C resulted in reduced capacitance density of 1.3 nF/cm^2 and 4 nF/cm^2 for ceramic-in-polymer and ceramic-in-insulator systems respectively. However, thermal treatment shifted the dielectric relaxation of the capacitors in the higher frequency. Particularly, ceramic-in-polymer capacitors showed a resonance frequency close to 410 MHz with a low loss tangent of 0.07 up to 200 MHz. The frequency-independent capacitor functions have been attributed to the nanometric interfacial polarization effects and the enhanced polymer permittivity. We have considered possible role of interplay of corresponding polarization mechanisms of the dielectric elements in minimizing the ferroelectric losses and capacitor functions in the high frequency. The fabricated nanodielectric composite capacitors have potential for various high-frequency applications in advanced miniature electronic devices. More fundamental studies are underway to understand the individual effects of micro-structure changes and existing impurities, particularly polymer matrix degradation during annealing on the filling factor and dielectric response of the composites.

Acknowledgments: Part of this work was conducted at the University of Alaska, Fairbanks with financial support from Defense Microelectronics Activity (DMEA) under grant No. H94003-05-2-0501 and SPAWAR-DARPA Grant No. N66001-07-1-2001. The work at NRL was supported by the Office of Naval Research. The work at the University of Oklahoma was supported by the NSF CAREER grant No. CHE-0239803 and the Center for Physics in Nanostructures, NSF MRSEC No. DMR-0520550.

References and Notes

1. T. J. Lewis, *IEEE Trans. Dielectr. Electr. Insul.* 11, 739 (**2004**).
2. E. Tuncer, I. Sauers, D. R. James, A. R. Ellis, M. P. Paranthaman, A. Goyal, and K. L. More, *Nanotechnology* 18, 325704 (**2007**).
3. J. K. Nelson and Y. Hu, *J. Phys. D: Appl. Phys.* 38, 213 (**2005**).

Delivered by Ingenta to: University of Notre Dame IP: 129.74.250.107 Wed, 24 Feb 2010 16:37:53

4. J. E. Garcia, R. Pérez, and A. Albareda, *J. Phys. D* 34, 3279 **(2001)**.
5. A. Biswas, I. S. Bayer, P. C. Karulkar, A. Tripathi, D. K. Avasthi, M. G. Norton, and J. B. Szczech, *Appl. Phys. Lett.* 91, 212902 **(2007)**.
6. Q. Tan, P. Irwin, and Y. Cao, *IEE J. Trans. Fund. and Mater.* 126, 1153 **(2006)**.
7. S. R. Ekanayake, M. B. Cortie, and M. J. Ford, *Curr. Appl. Phys.* 4, 250 **(2004)**.
8. P. Murugaraj, D. Mainwaring, and N. Mora-Huertas, *J. Appl. Phys.* 98, 054304 **(2005)**.
9. S. K. Saha, M. DaSilva, Q. Hang, T. Sands, and D. B. Janes, *Nanotechnology* 17, 2284 **(2006)**.
10. J. Xu and C. P. Wong, *J. Appl. Polym. Sci.* 103, 1523 **(2007)**.
11. A. Biswas, H. Eilers, F. Hidden, O. C. Aktas, and C. V. S. Kiran *Appl. Phys. Lett.* 88, 013103 **(2006)**.
12. Y. Kobayashi, A. Nishikata, T. Tanase, and M. Konno, *J. Sol–Gel Sci. Technol.* 29, 49 **(2004)**.
13. A. Biswas, I. S. Bayer, B. Marken, T. D. Pounds, and M. G. Norton, *Nanotechnology* 18, 305602 **(2007)**.
14. N. Nuraje, K. Su, A. Haboosheh, J. Samson, E. P. Manning, N.-L. Yang, and H. Matsui, *Adv. Mater.* 18, 807 **(2006)**.
15. C .B. Jiang, B. Wu, Z. Q. Zhang, L. Lu, and S. X. Li, *Appl. Phys. Lett.* 88, 093103 **(2006)**.
16. R. Hua, C. Zang, C. Shao, D. Xie, and C. Shi, *Nanotechnology* 14, 588 **(2003)**.
17. J. Yu, Y. Arai, T. Masaki, T. Ishikawa, S. Yoda, S. Kohara, H. Taniguchi, M. Itoh, and Y. Kuroiwa, *Chem. Mater.* 18, 2169 **(2006)**.
18. B. Hou, Z. Li, Y. Xu, D. Wu, and Y. Sun, *J. Electroceram.* 16, 127 **(2006)**.
19. V. Švorcik, J. Kralova, V. Rybka, J. Plesek, J. Červena, and V. Hnatowicz, *J. Poly. Sci. Part B: Polym. Phys.* 39, 831 **(2001)**.
20. K. Adachi and T. Kotaka, *Prog. Polym. Sci.* 18, 585 **(1993)**.
21. F. Wang, S. Liu, and C. Zhang, *Microelectron. J.* 38, 259 **(2007)**.
22. M. Na and S. W. Rhee, *Organic Electronics* 7, 205 **(2006)**.
23. H. B. Gon and N. Veeraiah, *J. Mater. Sci.* 16, 2571 **(1981)**.
24. U. Intatha, S. Eitssayeam, K. Pengpat, K. J. D. MacKenzie, and T. Tunkasiri, *Mater. Lett.* 61, 196 **(2007)**.

Received: 28 April 2009. Accepted: 30 June 2009.

Delivered by Ingenta to:
University of Notre Dame
IP : 129.74.171.77
Wed, 24 Feb 2010 16:57:05